BaBar Note # **295**
May 16th, 1996

Thermal Finite Elements Analysis of the BaBar Silicon Vertex Tracker

D. Barni, D. Giugni, F. Lanni, F. Palombo
Dipartimento di Fisica dell'Università and Sezione INFN, Milano, Italy

Abstract

In this note we present finite elements calculations of the thermal behavior of the BaBar silicon vertex tracker. Layers 1-2, 3 and 5 have been studied. Results show the adequacy of the cooling system in keeping the front-end chips into their optimal working condition. Thermo-mechanical results of layers 1-2 are also presented.

1 Introduction

The BaBar Silicon Vertex Tracker (SVT) consists of 5 silicon detectors layers[1]. Signals are taken out from detectors to front-end chips on the High Density Interconnect (HDI) [2]. This hybrid is hold by small feet on the cooling ring where a water flow of about 150cc/min assures the cooling. HDIs are then part of the thermal interface between chips and cooling system. Three types of hybrid will be used in BaBar SVT, differing in the number of chips (from 10 to 20) mounted on hybrid. Each chip has 128 channel with a power dissipation of about 3 mW / channel. Because of the maximum chip operating condition of about 40°C, we have verified, by Finite Elements Analysis (FEA), the efficiency of the cooling system in the whole configuration of the BaBar SVT. Due to the high precision request to BaBar SVT, the thermal field produced by electronic power generation can drive a not negligible deformation of the system. To evaluate this effect we realized a thermo-mechanical FEA for layers 1-2. The FEA has been checked and tuned by comparing its calculations with experimental measurements with a mockup test realized at the Lawrence Berkeley National Laboratory (LBNL).
The FEA analysis has been carried out using the code ANSYS 5.1[3].
In the Appendix A we present the essential of the theory used in the analysis.

2 FEA analysis of layers 1-2

2.1 Model description in thermal analysis

The model (see fig. 1), used for the thermal analysis, represents an half shell of one cooling ring of layers 1-2. It includes the cooling ring where the water flows, the feet keeping the HDI over the ring and allowing the cooling and two HDIs over each feet pair.

Water: It flows into the system from the top to the bottom and it has an inlet temperature of about 8 °C. We have supposed that there shouldn't be thermal gradient along radial direction of cooling channel. In real world this is caused by the mixing of water while it runs into the channel. To simulate this effects we have modified the water radial thermal conductivity to a value that guarantees good thermal diffusion (see section 4). Note that water is felt by the code as an anisotropic material. Heat exchange

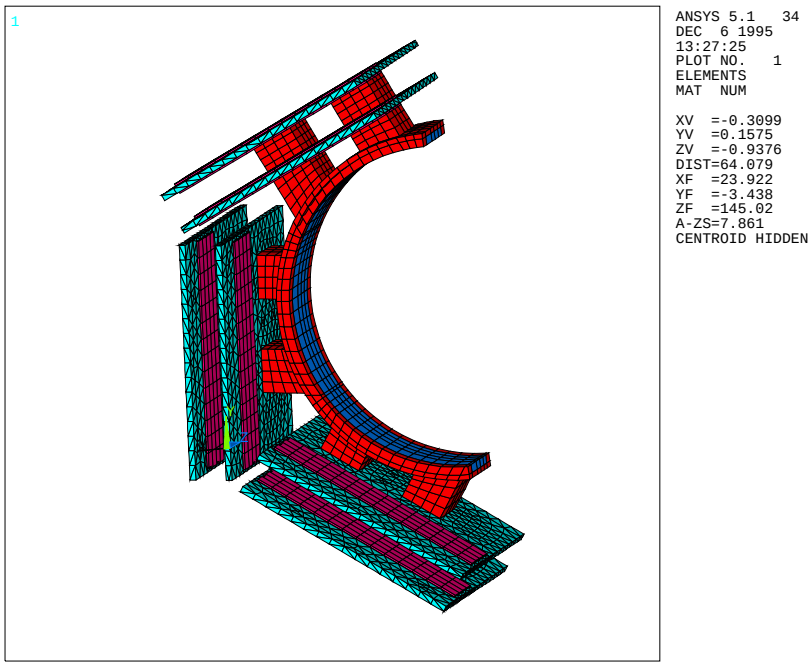

Figure 1: Model layers 1-2 with cooling ring , feet , HDIs and chips: water flows from the top to the bottom providing the heat exchange. Note the 2 HDIs on each pair of feet.

between water and cooling walls has been made by convective-link-element (see section 4).

Cooling ring and feet: Modeling this part of the structure we have tried to include all details that could modify the capability of the ring to take away the heat generated on the hybrid. We have realized that lateral walls of the channel help the heat exchange between water and the channel itself , making the heat exportation more efficient. To model this situation we use an element which can support mass transport effects. The possibility to add radial or transversal velocity to simulate water mixing is not practicable because of instability in the solution process. Water mixing can be simulated by modifying radial and transversal conductivities.

Hybrid: Substrate is made by alluminium nitrite[2] to guarantee good heat transfer. We suppose a perfect thermal link to the feet. The 7 chips on each side are represented as a single block. Chips are isolated from the substrate by a 100 μm layer to allow the chip power supply. The model built for this first simulation has no geometrical approximations in the sense that all volumes have been built as they are; this fact has produced a model with a lot of thetraedrum elements in the zone of the hybrid-substrate where a *mapped*[1] mesh would have generated many elements with bad aspect ratio[2] producing a less accurate solution. However once we have obtained the results with this model we can try to simplify some parts of it, having the possibility to check new results with the ones found with the complete model.

Loads: Only thermal loads have been applied to the system. The heat generation in the chip is at a rate of 3mW per channel and 128 channels per chip. Inlet water at 8°C and the rate of 150 cc/min give the constraint for heat diffusion. No convection effects between HDI and air have been included; this for the following reasons:

1. It is easy to apply convection to a FEA model but the coefficient describing this effect is very floating (even by a factor 20) vs. parameters which are not easily under control (humidity of air, air motus, orientation of the surface). The estimated amount of heat involved in the convective process is negligible with respect to the part taken away by the water. In fact the hybrid and air temperatures are quite close.

2. The situation in which all the heat generated has to be taken out by cooling water represents the worst case.

2.2 Thermal analysis results

We have obtained the thermal field produced by electronic system and cooling water. The maximum temperature is reached on the hybrid that is the nearest to the outlet cooling water. Results show that this maximum temperature is about 24.5°C.

[1] With squared and regular elements which keep the FEA model smaller.
[2] One dimension dominant with respect to the other

2.3 Thermo-mechanical analysis

Due to the high precision needed in the position of the SVT the thermal field can induce not negligible deformation to the layout of the detectors. The system made by end-pieces[3], ribs and detectors can also act like displacement amplifier. Once we have found the thermal field produced by electronics we can investigate how this field will modify the whole half shell.

2.3.1 FEA model

We simplified the model used for pure thermal analysis to be able to add modules and ribs without exceeding the limitations imposed by our code. The most important simplification has been carried out by the substitution of volumes that form the HDI substrate with a plane structure that will be meshed by shells[4]. This simplification reduced the total number of elements in the model. However we could not add all the half shell to the model because the estimated number of elements was still too high. We have chosen to simulate only the forward half shell and we have applied symmetry boundary condition to represent all the barrel. End-pieces , ribs and detectors have been added to the model. In order to find the deformation produced by the thermal field we suppose that the SVT is built at nominal temperature of about 20 °C.

2.3.2 Results.

Thermal field found on this model is very close to that one found with the previous thermal model. The approximation introduced by shell elements is negligible (in simulation for layer 3 and 5 we will use directly shell elements). Deformation found in this simulation (fig.2) shows that cooling ring is collapsed on itself, producing also a twist of the module (due to the different length of the feet). The maximum displacement is about 12 μm which is larger than the gravity deformation [4].

[3] Kevlar objects used to connect ribs to the cooling feet

[4] Shell is a 3D plane structure which we can add a thickness to

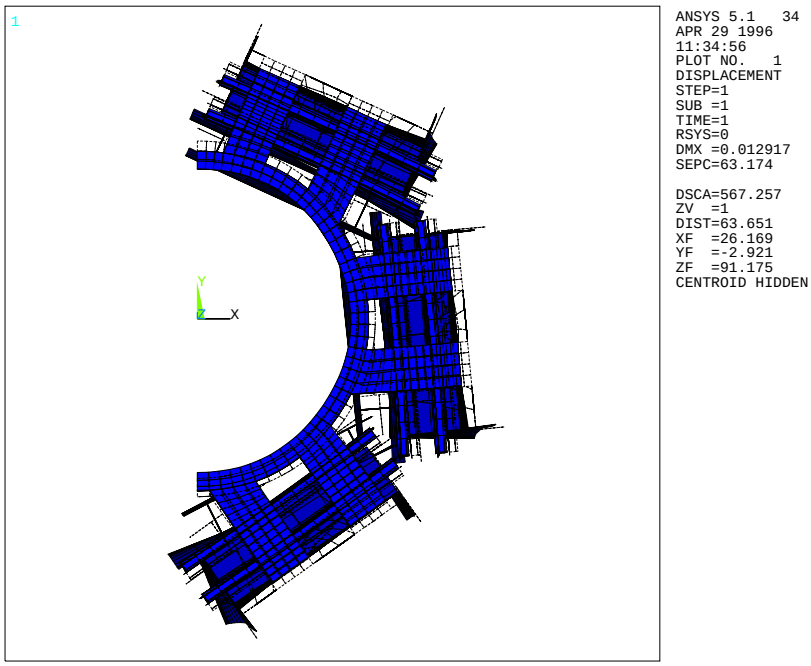

Figure 2: Layers 1-2: in full color the deformed shape while in dashed the original one. Note that the scale is enanched to let an easy view of the deformation.

3 Thermal analysis on layers 3 and 5

In the BaBar SVT three HDI types are used : one for layers 1-2 with 7 chips on each side, another one with 10 chips on each side for layer 3 and a third one with 5 chips in each side for layers 4 and 5. Due to this fact it is not easy to predict which layer is the most critical one. We considered then a different model for each of them.
The models used to simulate these layers are quite similar to those used previously for the thermal analysis.

In layer 3 we have simulated half backward cooling ring (fig.3) with its three hybrids. The model parameters are the same used in the simulation of the layers 1-2.
Layers 4 and 5 have HDIs with 5 chips on each side. Both layers have a cooling channel with the same geometry (dimension) and the same thermal

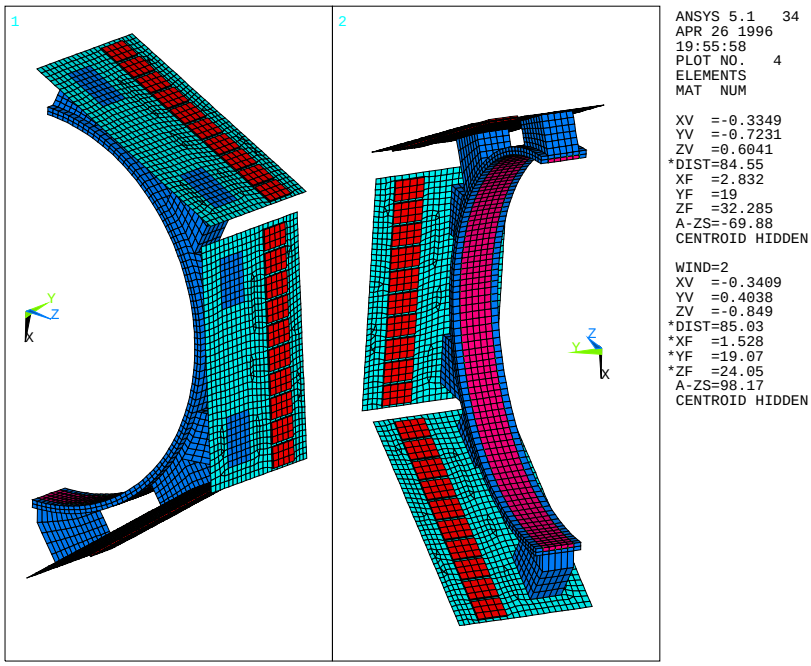

Figure 3: Layer 3 model: the water flows from the top to the bottom in the round channel. HDIs , with 10 chips on each side, are hold by 2 small feet on the cooling ring.

characteristics (water flow). The main difference is in the number of hybrids on the half shell (9 on the 5th layer and 8 on the 4th). Due to this reason we have decided to study only the 5th layer which is more critical than the layer 4.

3.1 Results

Layer 3 , where we have the maximum heat dissipation on single hybrid, will have a maximum temperature of about 24.5 °C.
On layer 5 the temperature in the hottest part of the hybrid near the outlet cooling water is about 22.5 °C. The temperature field in the different hybrids is quite the same while there is a temperature offset between hybrids near inlet cooling water and hybrids near outlet cooling water.
In Tab.1 we have summarized the results found for the studied layers. We

Region	ΔT ($^{\circ}C$)		
	Layer 1-2	Layer 3	Layer 5
Water - Feet	7.0	3.5	2.0
Feet - HDI	3.5	2.0	2.0
HDI - hottest-chip	6.0	11.0	10.5

Table 1: Temperature drops in three different regions of layers 1-2, 3 and 5.

have considered three regions of the thermal path between chips and cooling water: first region take into consideration the thermal drop in the interface between water and cooling channel wall, second refers to the drop due to the feet and third to the drop in the HDI substrate.

4 Cooling Test

The weakest point in the presented simulations is the part describing the heat exchange with the water channel. To check this point a test has been realized by LBNL. Experimental measurements have been done with a mockup (similar to the cooling ring of layers 1-2). A FEA has been run, including the same working conditions of the experimental LBNL measurements. In fig.4 we show experimental points and calculated ones. The agreement is fairly good. Measuring the temperature on 6 points, the cooling efficiency has been estimated. The most important effect in heat exchange between liquid and solid surfaces is the laminar boundary layer which plays a role on the temperature drop. This is simulated by a specific element called "convective link" (see appendix A).
Tuning the laminar coefficient of the convective link element we can control the temperature offset. Particular attention has been spent in the simulation of the water:

1. Water has been represented by solid elements with anisotropic characteristics. This is necessary to apply mass transport effects (represented as a mean water speed in the direction of the channel) and to simulate water mixing in radial and lateral direction.

2. We applied a convective link element between each node of water boundary and the correspective node in the cooling-ring-wall.

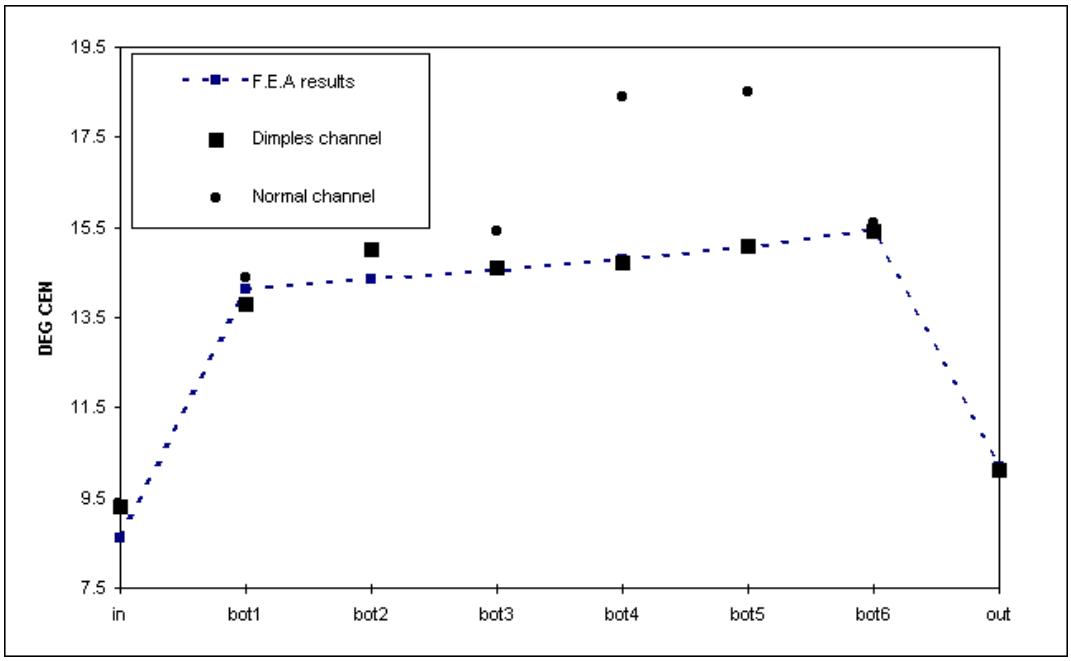

Figure 4: Squared dots are experimental data for channel with dimples while the dashed line is the FEA results. Circular dots show the temperature in a channel without dimples: note the temperature bump due to the water boundary layer oscillation.

The simulated points in fig 4 has been obtained by using the following parameters:

1. Laminar coefficient $h_f = 5.4$ mW/$(mm^2\,°\mathrm{C})$: This value is quite far from the values usually reported in literature for heat exchange between water and a metal. This is probably due to the geometrical shape of the channel (which has one dominant dimension) and to dimples (which have been provided in the test to increase the cooling efficiency) .

2. Water thermal radial conductivity K = 20.0 $W/(mm\,°\mathrm{C})$: With this radial conduction coefficient we obtained no thermal gradient in the

cooling channel section: this means that the dimples are effective in breaking the laminar flow.

5 Conclusion

We have studied the thermal behavior of the BaBar SVT HDI in its working condition. Results show that the SVT has sufficient cooling properties keeping chips in right temperature range. Because of the maximum chip operating condition of about 40 $^{\circ}C$ we are quite sure that HDI and chips will work in appropriate way even if the inlet temperature water will be higher than $8^{\circ}C$.
Termomechanical analysis on layers 1-2 points out that a maximum deformation of $\sim 12\mu$m .
The FEA pictures used to extract results presented in this note can be found at the FEA section of the BaBar Milan Web page: http://sunbabar.mi.infn.it

A Theory

A.1 Heat diffusion equation in F.E.

The first law of thermodynamics states that thermal energy is conserved. Specializing this to a differential control volume we have:

$$\rho\, c \left(\frac{\partial T}{\partial t} + \{v\}^T \{L\} T \right) + \{L\}^T \{q\} = \dot{q} \tag{1}$$

where:

- ρ = density
- c = specific heat
- t = time
- T = temperature (= T(x,y,z,t))
- $\{L\} = \left\{ \begin{array}{c} \frac{\partial}{\partial x} \\ \frac{\partial}{\partial y} \\ \frac{\partial}{\partial z} \end{array} \right\}$ = vector operator
- $\{v\} = \left\{ \begin{array}{c} v_x \\ v_y \\ v_z \end{array} \right\}$ = velocity vector for mass transport of heat
- $\{q\}$ = heat flux vector
- $\dot{q}$ = heat generation rate per unit volume

Next , Fourier's law is used to relate the heat flux vector to the thermal gradients:

$$\{q\} = -[D]\{L\}\, T \tag{2}$$

where:

- $[D] = \left[\begin{array}{ccc} K_{xx} & 0 & 0 \\ 0 & K_{yy} & 0 \\ 0 & 0 & K_{zz} \end{array} \right]$ = conductivity matrix
- K_{xx}, K_{yy}, K_{zz} = conductivity in the element x, y and z directions.

Combining equations (1)and (2) we have:

$$\rho \cdot c \left(\frac{\partial T}{\partial t} + \{v\}^T \{L\} T \right) = \{L\}^T \left([D] \{L\} T \right) + \dot{q} \tag{3}$$

expanding equation 3 we found its more familiar form:

$$\rho \cdot c \left(\frac{\partial T}{\partial t} + v_x \frac{\partial T}{\partial x} + v_y \frac{\partial T}{\partial y} + v_z \frac{\partial T}{\partial z} \right) =$$
$$\dot{q} + \frac{\partial}{\partial x} \left(K_x \frac{\partial T}{\partial x} \right) + \frac{\partial}{\partial y} \left(K_y \frac{\partial T}{\partial y} \right) + \frac{\partial}{\partial z} \left(K_z \frac{\partial T}{\partial z} \right)$$

Three types of boundary condition are considered:

1. Specific temperature acting over surface S_1:
   $T = T^*$
   where T^* is he specified boundary temperature

2. Specified heat flows acting over surface S_2:
   $\{q\}^T \{\mu\} = -q^*$
   where:

   - $\{\mu\}$ = unit outward normal vector.
   - q^* = specified heat flow.

3. Specified convection surfaces acting over surface S_3:
   $\{q\}^T \{\mu\} = -h_f \left(T_B - T \right)$ where:

   - h_f = film coefficient at temperature $(T_B + T_S)/2$.
   - T_B = bulk temperature of adjacent fluid.
   - T_S = temperature at the surface of the model.

Combining equation(2) with equations from boundary condition, we have:

$$\{\eta\} [D] \{L\} T = q^* \tag{4}$$
$$\{\eta\}^T [D] \{L\} T = h_f \left(T_B - T \right) \tag{5}$$

Premultiplying equation (3) by a virtual change in temperature, integrating over the volume of the element and combining with equation (4) and (5) with some manipulation yields:

$$l \int_{vol} \left(\rho \, c \, \delta T \left(\frac{\partial T}{\partial t} + \{v\}^T \{L\} T \right) + \{L\}^T \delta T \left([D] \{L\} T \right) \right) d(vol) =$$
$$\int_{S_2} \delta T \, q^* d(S_2) + \int_{S_1} \delta T \, h_f \left(T_B - T \right) d(S_3) + \int_{vol} \delta T \dot{q} d(vol) \tag{6}$$

where:

- vol = volume of the elements
- δT = an allowed virtual temperature ($=\delta T(x, y, z, t)$)

T is allowed to vary in both space and time so we separate this dependency:

$$T = \{N\}^T \{T_e\} \tag{7}$$

where:

- $\{N\} = \{N(x, y, z)\}$ = element shape functions
- $\{T_e\} = \{T_e(t)\}$ = nodal temperature vector

With these considerations, the time derivatives may be written as

$$\dot{T} = \frac{\partial T}{\partial t} = \{N\}^T \{\dot{T}_e\} \tag{8}$$

while δT has the same form as T:

$$\delta T = \{\delta T_e\}^T \{N\} \tag{9}$$

Introducing the matrix $[B] = \{L\}\{N\}^T$ the variational statement of equation(6) can be combined with equations (8-9) to yield:

$$\begin{aligned} l \int_{vol} \rho\, c \{\delta T_e\}^T \{N\}\{N\}^T \{\dot{T}_e\} d(vol) + \int_{vol} \rho\, c \{\delta T_e\}^T \{N\}\{v\}^T [B]\{T_e\} d(vol) + \\ + \int_{vol} \{\delta T_e\}^T [B]^T [D][B]\{T_e\} d(vol) = \int_{S_2} \{\delta T_e\}^T \{N\} q^* d(S_2) + \\ + \int_{S_3} \{\delta T_e\}^T \{N\} h_f \left(T_B - \{N\}^T \{T_e\}\right) d(S_3) + \int_{vol} \{\delta T_e\}^T \{N\} \dot{q} d(vol) \end{aligned} \tag{10}$$

Assuming now:

- ρ is constant over the volume of the element.
- c and $\dot{q}$ may vary over the element.
- $\{T_e\}$, $\{\dot{T}_e\}$ and $\{\delta T_e\}$ are nodal quantities and do not vary over the element.

Since all quantities are premultiplied by an arbitrary vector $\{\delta T_e\}$, it may be dropped from the resulting equation that now can be reduced to:

$$[C_e^t]\{\dot{T}_e\} + \left([K_e^{tm}] + [K_e^{tb}] + [K_e^{tc}]\right)\{T_e\} = \{Q_e\} + \{Q_e^c\} + \{Q_e^g\} \qquad (11)$$

where:

- element specific heat:
  - $[C_e^t] = \rho \int_{vol} c\{N\}\{N\}^T d(vol)$
- total element conductivity matrix
  - $[K_e^{tm}] = \rho \int_{vol} c\{N\}\{v\}^T [B] d(vol)$
  - $[K_e^{tb}] = \int_{vol} [B]^T [D][B] d(vol)$
  - $[K_e^{tc}] = \int_{S_3} h_f \{N\}\{N\}^T d(S_3)$
- total element heat flow vector
  - $\{Q_e^f\} = \int_{S_2} \{N\} q^* d(S_2)$
  - $\{Q_e^c\} = \int_{S_3} T_B h_f \{N\} d(S_3)$
  - $\{Q_e^g\} = \int_{vol} \dot{q}\{N\} d(vol)$

A.2 Elements used in FEA simulation.

A.2.1 Solid 3D: Thermal Solid

Solid has three-dimensional thermal conduction capability. The element has eight nodes with single degree of freedom, temperature, at each node. This element also can compensate for mass transport heat flow from a constant velocity field but, in this case, temperatures should be specified along the entire inlet boundary to assure a stable solution. This element follows the matrices and load vectors of a general thermal analysis as we have discussed in previous paragraph.

Mass transport effect This effect is included as described in equation 1. The solution accuracy is measured in term of a non-dimensional criteria called the element Peclet number

$$P_e = \frac{V\ L\ \rho\ C_p}{2\ K} \qquad (12)$$

where:

- V = magnitude of the velocity vector
- L = element length along the velocity vector direction
- ρ = density of the fluid
- C_p = specific heat of the fluid
- K = equivalent thermal conductivity along the velocity vector direction.

For the solution to be physically valid, the following condition has to be satisfied

$$P_e < 1 \tag{13}$$

This check is carried automatically during the element formulation.

A.2.2 Shell: Thermal Shell

Shell is a three-dimensional element having in-plane thermal conduction capability. The element has four nodes with single degree of freedom (temperature) at each node. The element may have variable thickness. The thickness is assumed to vary smoothly over the area of the element with the thickness input at the four nodes. This elements follows the matrices and load vectors of a general thermal analysis as we have discussed in previous paragraph.

A.2.3 Link (Convection link)

Link is a uniaxial element with the ability to convect heat between its nodes. The element has a single degree of freedom, temperature, at each node point. The element conductivity (convection) equation is

$$A\, h_f^{eff} \begin{bmatrix} 1 & -1 \\ -1 & 1 \end{bmatrix} \{T_e\} = \{Q_e\} \tag{14}$$

where:

- A = area over which element acts
- h_f^{eff}=effective film coefficient; in our case we fix it = h_f

- $\{T_e\}$ = nodal temperature vector = $\{T_e(t)\}$
- $\{Q_e\}$ = element heat flow vector

The quantity $K_e^t = A\, h_f^{eff} \begin{bmatrix} 1 & -1 \\ -1 & 1 \end{bmatrix}$ is the convection matrix. Note that no shape function is used, so nodes may be coincident.

References

[1] D. Boutigny et al, *"BaBar Technical Design report", SLAC-R-95-457, March 1995*

[2] D. Giugni at al, *"Hybrid Design of the BaBar Silicon Vertex Tracker" BaBar Note 240, July 1995*

[3] Ansys revision 5.1, Svanson Analysis System Inc.

[4] D. Barni at al, *"Mechanical Finite Elements Analysis of the BaBar Silicon Vertex Tracker " BaBar Note 296, May 1996*